Songklanakarin J. Sci. Technol.
33 (1), 51-60, Jan. - Feb. 2011

SJST SONGKLANAKARIN JOURNAL OF SCIENCE AND TECHNOLOGY
http://www.sjst.psu.ac.th

Original Article

Simulation of leading edge cavitation on bulb turbine

Thaithacha Sudsuansee[1]*, Udomkiat Nontakaew[1] and Yodchai Tiaple[2]

[1] *Department of Mechanical and Aerospace Engineering, King Mongkut's University of Technology North Bangkok, Bang Sue, Bangkok, 10800 Thailand.*

[2] *Naval Architecture and Marine Engineering, International Maritime College, Kasetsart University, Si Racha Campus, Si Racha, Chon Buri, 20230 Thailand.*

Received 20 July 2010; Accepted 25 February 2011

Abstract

Cavitation caused by phases exchange between fluids of large density difference occurs in a region where the pressure of water falls below its vapor pressure. The density of water in a water-vapor contact area decreases dramatically. As a result, the flow in this region is compressible, which affects directly turbulent dissipation structures. Leading edge cavitation is naturally time dependent. Re-entrant jet generated by liquid flow over a cavity is a main actor of cavity shedding. Simulation of unsteady leading edge cavitation flows through a 4-blade runner bulb turbine was performed. Particular attention was given to the phenomena of re-entrant jet, cavity shedding, and cavitation vortices in the flow over turbine blade. The Reynolds-Average Navier-Stokes equations with finite volume discretization were used. The calculations were done with pressure-based algorithms since the flow possesses a wide range of density change and high complexity turbulence. The new formula for dilatation dissipation parameter in k-ω model was introduced and the turbulent Mach number was calculated from density of mixture instead. 2-D and 3-D hydrofoils based on both numerical and experimental results accomplished a validation. The results show that re-entrant jet, shedding of cavity, and cavitation vortices can be captured. In addition, this paper also calculates the cycle frequency of torque generated by the runner and vapor area evolution on the blade surface. The cycle frequency varies with cavitation number. At normal operation of this turbine ($\sigma = 1$) it is found that both of them have a frequency of 46 Hertz.

Keywords: cavitation, turbulent, computational fluid dynamics, dilatation dissipation, bulb turbine

1. Introduction

Cavitation is a serious problem for water turbine developers. The cavitation may cause noise pollution, erosion on the blade surface and the wall of the turbine, and a decrease of the water turbine efficiency (Avellan, 2004). Cavitation occurs in the flow of water when owing to regions of high flow velocity and the local static pressure decreases below the vapor pressure. Incipient cavitation is simple to calculate as one just has to find the lowest pressure that indicates the inception of the cavitation once this lowest pressure reaches the vapor pressure. Cavitation may occur on the blade suction surface in region of low pressure or at the runner leading edge at off-design operation. Experimental and numerical studies both identically indicate that the efficiency of a turbine strongly decreases when the value of cavitation number is less than the critical one. The real challenge for cavitation simulation is to simulate full cavitating flow, which in most case requires the calculation of two-phase flow including phase change from water to vapor and vice versa.

This paper focuses on numerical studies of time dependent characteristics of cavitation flow on the leading edge of a turbine blade with high flowing rate. According to the experimental results of Grekula and Bark (2001), the behavior

* Corresponding author.
Email address: ttc_sss@hotmail.com

of leading edge cavitation comprises re-entrant jet, cavity deformation, and cavitation vortices. The unsteady cavitation flow is characterized by the frequency shedding of the bubble cloud caused by the development of a re-entrant jet (Franc and Michel, 2004). Computational fluid dynamics (CFD) analysis is very helpful to predict flow fields, the efficiency for the different propeller curves, vibration, and cavitation erosion of material. The use of CFD brought further substantial improvements in hydraulic design, in the detailed understanding of flows, and its influence on turbine performance.

The mixture model (Kubota *et al.*, 1992) for the water-cavity two-phase flow analysis together with the k-ω turbulent model provides a good result for 2-D/3-D steady and 2-D unsteady cavitation flows. This mixture model includes the term of interphase mass transfer, which was derived from the well-known Rayleigh-Plesset equation of cavitation bubble dynamics. The problem occurs when this model is applied to 3-D unsteady flow, there is no shedding of cavity. Coutier *et al.* (2003) gave an explanation that the incorrect flow was caused by the lack of term, which represented the compressibility effect in the turbulence model. Wilcox (2004) proposed the k-ω model by including the effect of fluid compressibility of single phase. In this study, however, the turbulent model needs to be more modified in order to take into account the two-phase flow. This paper proposes the new idea for evaluating the turbulent Mach number using volume fraction.

The calculations are tested on 2-D and 3-D hydrofoil. The 2-D case was validated with both experimental (Arndt *et al.*, 2000) and numerical (Koop, 2008) results. The 3-D case was validated with experimental result of Foeth and Terwisga (2006).

2. Cavitation Model

The homogeneous multiphase transport equation based model is applied in this study. The advantage of this model is its ability to change the phase using the transport equation, which can give the calculation result for explaining the physical cavitation flow consisting of cavity detachment and cavity closure. In continuity equation, there is the source term for exchanging phase between liquid and vapor. Several studies present the different types of the source term. All of them are the presentation of an empirical factor to be applied to the mass transfer adjustment. These factors are the results of experimental and numerical calibration. This source term derives from the equation of Rayleigh-Plesset (RP) (Kubota *et al.*, 1992) supposing that the thermal equilibrium is between the liquid phase and the vapor phase. The equation is based on the control of the evaporation and condensation of the water.

The continuity equation, equation of classical RANS, and the fluid flow mixing homogeneously are shown below.

$$\frac{\partial \rho_m}{\partial t} + \vec{\nabla} \cdot \left(\rho_m \vec{C}_m \right) = 0 \tag{1}$$

$$\frac{\partial}{\partial t}\left(\rho_m \vec{C}_m \right) + \rho_m \left(\vec{C}_m \cdot \vec{\nabla} \right) \vec{C}_m = -\vec{\nabla}\left(p_m \right) + \vec{\nabla}\left(\bar{\bar{\tau}} + \bar{\bar{\tau}}_t \right) + \vec{M}_m + \vec{f} \tag{2}$$

$$\frac{\partial \alpha_n \rho_n}{\partial t} + \vec{\nabla} \cdot \left(\alpha_n \rho_n \vec{C}_m \right) = \Gamma_n \tag{3}$$

The cavitation process is comprised of three components supposed to have no slipping between the phases that consist of vapor (v), water (w), and non-condensable gas in the form of micro-scaled bubbles called nuclide (nuc). Stoichiometry of each component described by a scalar of the volume fraction as follows:

$$\left(\alpha_w + \alpha_{nuc} \right) + \alpha_v = 1 \tag{4}$$

As for the cavitation problem, the phase of the non-condensable gas supposed to homogeneously mix with the phase of liquid by the invariant volume fraction α_{nuc}. In this hypothesis the fractions α_w and α_{nuc} are able to plus into volume quantity α_l or the equation of $\alpha_w + \alpha_{nuc} = \alpha_l$ and use α_l to calculate in the transport equation. The main equation of liquid phase consisting of non-condensable gas is

$$\frac{\partial}{\partial t}\left(\alpha_l \rho_l \right) + \vec{\nabla} \cdot \left(\alpha_l \rho_l \vec{C}_m \right) = \Gamma_l = \dot{m}_l^v + \dot{m}_l^c \tag{5}$$

$\alpha_v = 1 - \alpha_l$ and $\dot{m}_l^v, \dot{m}_l^c$ are the source terms of vaporization and condensation, respectively (bubble growth and collapse), which their unit is $kg/m^3/s$ with mass exchange between vapor and liquid during the cavitation occurrence.

The cavitation model based on the equation of Rayleigh-Plesset is applied to cavitation rate estimation. While the bubbles begin to form in that liquid, dynamics of the bubbles can be explained by the RP equation supposing that the term of viscosity and surface tension have substantial value as follows:

$$\rho \left[R\ddot{R} + \frac{3}{2}\dot{R}^2 \right] = p_v - p \tag{6}$$

$$\Gamma_l = N \rho_l 4\pi R_o^2 \dot{R} \tag{7}$$

R is a bubble radius, p_v is a vapor pressure of the bubble, p is a pressure in liquid, and ρ_l is a liquid density. The calculation by first order approximation is applied to the term of bubble growth and collapse in the RP equation without calculating the term in the higher order since the frequency of the vibration is low and neglect the interaction term between the bubbles. It can be explained by the following equation:

$$\dot{R} = \sqrt{\frac{2}{3} \frac{|p_v - p|}{\rho_l}} \tag{8}$$

The number of the bubbles per unit of fluid volume N is as follows:

Vaporization period

$$N^v = \frac{3\alpha_l \alpha_{nuc}}{4\pi R_0^3} \tag{9}$$

Condensation period

$$N^c = \frac{3\alpha_v}{4\pi R_0^3} \tag{10}$$

Practically, the vaporization and condensation have a different scale of term. Thus, the empirical literals F^c and F^v are in the equation to adjust the value to be practically similar. Due to the substitution in the Equation 8, 9, and 10 in the equation (7), there is

$$\dot{m}_l^v = -F^v \frac{3\rho_v \alpha_{nuc}\alpha_l}{R_0}\sqrt{\frac{2}{3} Max\left(\frac{p_v - p}{\rho_l}, 0\right)} \tag{11}$$

$$\dot{m}_c^v = -F^c \frac{3\rho_v (1-\alpha_l)}{R_0}\sqrt{\frac{2}{3} Max\left(\frac{p - p_v}{\rho_l}, 0\right)} \tag{12}$$

The non-condensable gas is supposed to be a round-shaped bubble in the volume of nucleation to apply to the cavitation process. The general value of α_g is 10^{-5} and a default value of the radius of the nuclide is $R_0 = 10^{-6}$ m. In the two-dimensional hydrofoil, the best value, which gives the result of the cavity, is $F^v = 50$, $F^c = 0.015$ (CFX-ANSYS, 2004).

3. Turbulence Model

In this study, Reynolds averaging equation and two equations of the $k-\omega$ turbulent transport equations are used for turbulence modeling. These $k-\omega$ equations developed from the $k-\varepsilon$ model were used in many aero- and hydrodynamic studies and can also be applied in complex flow at sub-layer and wall function grids. Turbulent viscosity is calculated from the ratio of turbulence kinetic energy and specific dissipation rate, $\mu_t = \rho_m (k/\omega)$. In the calculation of turbulence transport model, both vapor and liquid are supposed to be homogenous which is called "homogenous turbulence".

Turbulent kinetic energy

$$\frac{\partial k}{\partial t} + u_j \frac{\partial k}{\partial x_j} = \tau_{ij}\frac{\partial u_i}{\partial x_j} - \beta_w^* k\omega + \frac{\partial}{\partial x_j}\left[\left(\mu + \sigma_w^* \mu_t\right)\frac{\partial k}{\partial x_j}\right] \tag{13}$$

Turbulent dissipation rate

$$\frac{\partial \omega}{\partial t} + u_j \frac{\partial \omega}{\partial x_j} = \alpha_w \frac{\omega}{k}\tau_{ij}\frac{\partial u_i}{\partial x_j} - \beta_w \omega^2 + \frac{\partial}{\partial x_j}\left[\left(\mu + \sigma_w \mu_t\right)\frac{\partial \omega}{\partial x_j}\right] \tag{14}$$

$$\alpha = 5/9; \quad \beta = 3/40; \quad \beta^* = 9/100; \quad \sigma = 1/2; \quad \sigma^* = 1/2$$

$$\mu_t = \rho\frac{k}{\omega} \qquad \varepsilon = \beta^* \omega k \qquad L_t = \frac{k^{1/2}}{\omega}$$

4. Effect of Compressibility

The $k-\omega$ model for the flow with the Mach number over 5 can lead to the changes of the correct flow (Wilcox, 2004). It is caused by the inaccurate prediction of spreading rate, especially at the mixing layer, due to the increasing Mach number of the compressible fluid. The influence of the fluid compressibility can be explained by the relation of dissipation rate supposing the correlation between velocity-gradient fluctuations and kinematic viscosity fluctuation are neglected and the type of flow is homogeneous turbulence as shown in the following relation.

$$\bar{\rho}\varepsilon = \bar{\rho}\varepsilon_s + \bar{\rho}\varepsilon_d \tag{16}$$

with

$$\bar{\rho}\varepsilon_s = \bar{\nu}\,\overline{\rho\omega_i''\omega_i''} \text{ and } \bar{\rho}\varepsilon_d = \frac{4}{3}\bar{\nu}\,\overline{\rho u_{i,i}'' u_{i,i}''} \tag{17}$$

The quantity of ε_s is called solenoidal dissipation and the quantity of ε_d is called dilatation dissipation. However, the latter term can usually occur in case of the compressible fluid only.

The existing model is more accurate in case of the compressible flow by calculating the dilatation dissipation term by modifying the value of β_w and β_w^* in the k-ω model to be the function of turbulence Mach number of M_t^2 = $2k/A^2$ which can be shown as the following relation.

$$\beta_w^* = \beta_{wi}^*\left(1 + \xi^* F(M_t)\right) \text{ and } \beta_w = \beta_{wi} - \beta_{wi}^* \xi^* F(M_t)$$

$$\text{with } F(M_t) = \begin{cases} \left(M_t^2 - M_{t_0}^2\right) & \text{if } M_t > M_{t_0} \\ 0 & \text{if } M_t \le M_{t_0} \end{cases}$$

$$M_{t_0} = 0.25 \text{ and } \xi^* = 1.5 \tag{18}$$

5. Modified Turbulence Model

The reason why we have to modify the turbulence model is because the existing $k-\omega$ turbulence model cannot show the behavior of cavity shedding. Consequently, the turbulence model needs to be modified. As shown in Figure 1, the figure shows examples of the calculation result before modifying the turbulence model by modeling in the two-

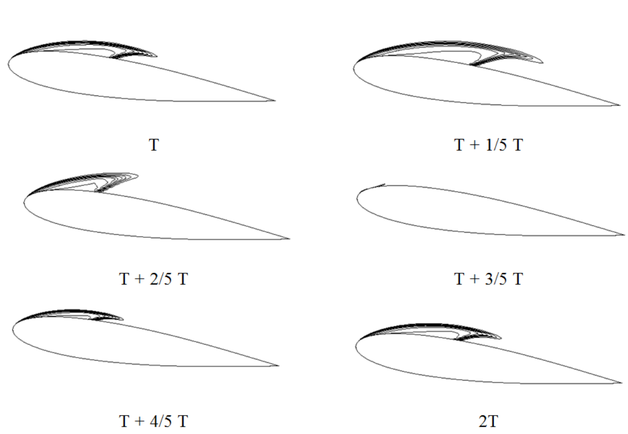

Figure 1. Simulation results before modifying the turbulence model.

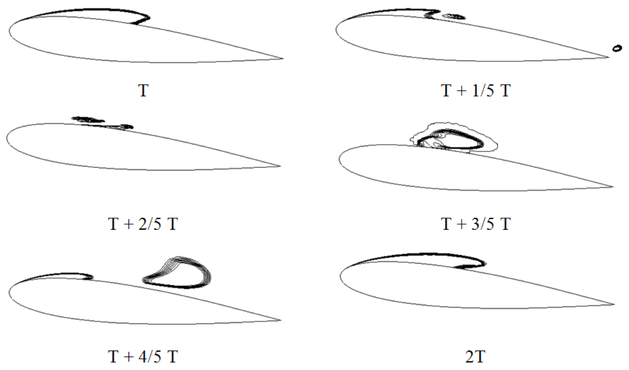

Figure 2. Simulation result after modifying the turbulence model.

dimensional hydrofoil. In addition, Figure 2 shows the result after modifying, which can show the behavior of cavity shedding changing according to time.

According to the related studies, there is another type of the flow, which has a behavior like compressible flow. It does not derive from one-phased compressed fluid but derives from phase change due to the cavitation phenomenon. When the phase changes, due to cavitation, between liquid (water) and gas (vapor), the density could be greatly change for 58,000 times, while the pressure shows little change. This effect causes a decrease of the speed of sound in the fluid as in the relation $A = \sqrt{\partial P / \partial \rho}$, which can be explained in Figure 3.

Based on the aforementioned flow characteristic, it can be applied for the multiphase flow model. The density can be considered by the mixture of two phases as shown in the following relation.

$$\rho_{mixture} = \frac{r_v \rho_v + r_l \rho_l}{r_v + r_l} = r_v \rho_v + r_l \rho_l \ \text{(for two phase flow)} \tag{19}$$

r_v, r_l = volume fraction of the vapor and the water respectively

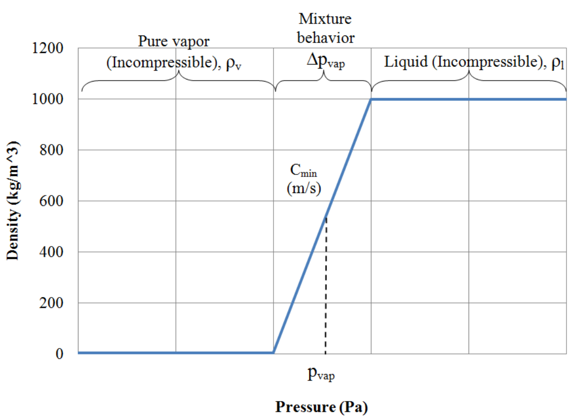

Figure 3. Diagram of phase transport caused by the cavitation.

ρ_v, ρ_l = density of the vapor and the water respectively

The speed of sound of the mixture in the two-phase flow model is shown in the following equation.

$$A_{mixture} = \frac{dp}{d\left(r_v \rho_v + r_l \rho_l\right)} \tag{20}$$

The great decrease in the speed of sound causing the flow to be supersonic. In this research, a k-ω turbulence model was modified by changing the speed of sound of compressible flow in terms of the turbulence Mach number to become mixed speed of sound caused by incompressible or little compressible flow, because a mix between water and vapor in the cavitating flow leads to a low value of speed of sound, especially at the interface of two phases as shown in the following relationship:

Turbulent mach number

$$M_{t,new}^2 = \frac{2k}{A_{mixture}^2} = \frac{2k}{\left(\dfrac{dp}{d\left(r_v \rho_v + r_l \rho_l\right)}\right)^2} \Leftarrow \textit{Modified equation for cavitation flow} \tag{21}$$

The modified-turbulent mach number represented in the turbulent model. Equations 21 can be used to simulate unsteady cavitation flow behaviors, especially cavitation shedding in three-dimensional complex geometry such as a runner turbine.

6. Computational Setup

The turbine in this study was designed and developed by Tiaple and Nontakaew (2004) for a hydro-power turbine of the Lower Mae Ping Dam, which basically proposed to be a pump storage of the eighth hydro-generator unit of Bhumibol Dam, Thailand. Each year, the quantity of water that passes through the Lower Mae Ping dam is about 150-500 m^3/s with an average head at 2.4 m.

In this simulation, CFX was selected to be the calculation tool for solving equations of unsteady flow through a 4-blade bulb turbine model with a size of 650 mm in diameter and with 15-guide vanes as shown in Figure 4 (at net head = 3.0 m and flow rate = 1.88 m^3/s). The hub and tip clearance of runner were ignored in this simulation.

The solver with a second-order scheme (Barth and Jesperson, 1989) was used in this study. A multi-block structured mesh was generated by TurboGrid mesh generator for hydraulic machines. Fine meshes were simulated in cavitation condition. The amount of nodes is adequate to capture cavitating flow characteristics. The computing domain corresponding to a single machine passage (1/4 of the machine), was made of O-blocks around the blade, H-blocks at the leading, and J-blocks at the trailing edge of the blade as shown in Figure 5

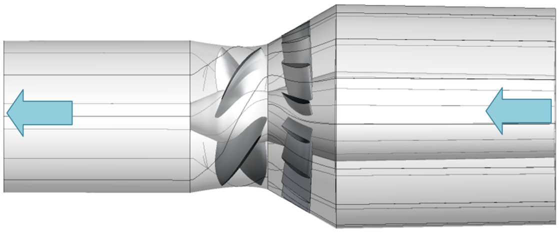

Figure 4. Bulb turbine.

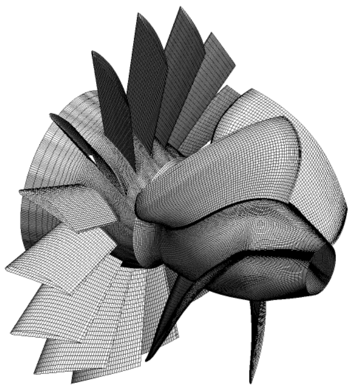

Figure 5. Runner turbine grid.

7. Boundary Conditions

Unsteady-state solutions were obtained for different regimes by setting the flow rate at the turbine inlet and the average static pressure at its outlet as boundary conditions (the net cavitation number value was set based on the outlet pressure and head of the turbine stage). Single channel geometry in rotating frame of reference was used and periodicity conditions were applied to the channel connections. The hub, the shroud, and the runner blade were set to rotating walls whereas the inlet and the outlet were set to stationary.

8. Numerical Method

In this research, commercial software, Ansys CFX (2004) was applied to calculate using the finite volume method. As for the transient term, it was discreted based on the second order backward Euler scheme, while coupling between pressure and velocity was made by using Rhie and Chow technique. For the advection term, the second order upwind difference scheme was used. The advection scheme for calculation is as follows:

$$\phi_{ip} = \phi_{up} + \beta \nabla \phi \cdot \Delta \vec{r} \tag{22}$$

whereas ϕ_{up} is an upwind node value and $\vec{r}$ is a vector value from upwind node at ip. $\nabla\phi$ is the control volume gradient of the upwind node. β is close to 1 as much as possible without creating local oscillations. β is computed based on the boundedness principle applied in the research of Barth and Jesperson (1989). This scheme is both accurate and bounded since it only reduces to first order near discontinuities

The time step used was 0.0001 s. A maximum numerical residual was kept below 10^{-4} as the convergence criteria. The cavitation model itself was configured with a non-condensable gas volume fraction of 5x10^4. It was believed that increasing the non-condensable gas volume fraction in the numerical model would increase the dynamics of the system. Thus, adding instability was not a problem in the study. The water vapor pressure P_v was set at 3,540 Pa. The cavitation number was adjusted by changing of reference pressure, P_{ref}, in the solver. The same effect could also be achieved by having a constant reference pressure and adjusting the vapor pressure.

A code for modification of the k-ω homogeneous turbulence model was added to the program in order to improve β and β^* to be more accurate in case of the calculation of cavitation flow by including compressibility effect.

9. Validation

In terms of validation, we tested the accuracy of the model by comparing calculated results with experimental results in simple shapes (2-D and 3-D hydrofoil) because they use less resource and save time in computing than the runner turbine, and many researches made about hydrofoil are reliable. Since validation was proven, the simulation of cavitation flow on a bulb turbine was calculated in the next step.

We compared results obtained from different turbulence models and analyzed the influence of grid resolution. The comparison was done in terms of cavity shedding and cycle frequency.

In two-dimensional hydrofoil comparison, we chose the NACA0015 model with 6^o angle of attack and a cord length of 0.13 m to compare it with Arndt's (2000) experiment and Koop's (2008) numerical calculation at inlet velocity = 12 m/s, pressure outlet = 74,200 Pa, free stream temperature = 293 K, water density = 998.2 kg/m^3, water sound speed = 1,537.6 m/s, and cavitation number = 1.

The numerical result can predict correct results of unsteady flows as shown in Figure 2. Since the suction side of the hydrofoil has very low pressure, water in that zone was changed into vapor at the surface of hydrofoil, called cavity. When the cavity became larger, re-entrant jet from downstream occurred. The influence of re-entrant jet causing the structure of cavity to be broken off and some part moved towards downstream called "cavity shedding" and it collapsed when it reached to a high pressure zone. At the same time, the new cavity formed became larger and the re-entrant jet occurred constantly according to the time. (Figure 6)

We also calculated with different turbulent models and different numbers of grid point on foil as shown in the table below.

From Table 1, k-ε and k-ω turbulent models can not be used to simulate cavity shedding. While SST (Shear Stress

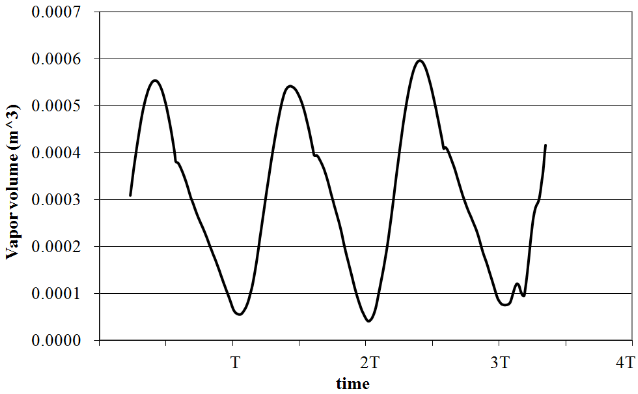

Figure 6. Vapor volume change over time.

Transport) model can only be used to simulate cavity shedding in case of higher number of grid on foil. But the modified model in this research can be used to simulate such behaviors even in case of lower number of grid on foil. However, error in calculating shedding frequency is higher when the lower number of grid is used.

In the three-dimensional case, we chose 3D twist hydrofoil at an angle of attack = -2°, cord length = 0.15 m by comparing with the experimental results of Foeth and Terwisga (2006). At inlet velocity = 50 m/s, pressure outlet = 1,375 kPa, free stream temperature = 297 K, and cavitation number = 1.1. The results are shown in Table 2.

The modified model can also be used to calculate cavity shedding results even in the three-dimensional geometry, which is more complex due to the additional influence of re-entrant jet in z-axis. Therefore, the number of grid point on foil should be high enough to capture cavity shedding and the calculation with a high performance computer is also necessary.

When taking into consideration flow accuracy, we found that the results were similar to Foeth and Terwisga (2006) experiment (Figure 7). The influence of re-entrant jet and side-entrant jet affected shedding of vortex cavity (like horse-shoes shape), which is called "cavitation vortices"

10. Simulation Results

The results of the modified turbulent model can be used to simulate cavitation flow in complex situation, e.g. bulb turbine. The flow behaviors in this simulation is also similar to Grekula and Bark (2001) experiment (Table 3).

In this study, we found that there were some vortices occurred at the cavity closure due to re-entrant jet. Figure 8 illustrates velocity vector plotted on the blade section at span 5% from the shroud wall. The re-entrant jet moved to the cavity structure. Its momentum is adequate for flowing to the leading edge of a blade and breaking off the cavity structure. The cavity shedding from the main group became vapor cloud and moved along with the main flow downstream and condensed when entering the high pressure region. Mean-

Table 1. Comparison of cavity shedding calculation with different turbulent model on two dimensional hydrofoil.

Turbulence Model	Number of grid point on foil	Results can capture Shedding	Shedding frequency (Hz)
k-ε	400	No	-
k-ω	400	No	-
SST	200	No	-
SST	400	Yes	32
Mod. Model	200	Yes	27
Mod. Model	400	Yes	21
Experiment (Arndt *et al.*, 2000)	-	-	16
Inviscid (Koop, 2008)	400	Yes	24

Table 2. Comparison of cavity shedding calculation with different turbulent model on three dimensional hydrofoil.

Turbulence Model	Number of grid point on foil	Results can capture Shedding	Shedding frequency (Hz)
k-ω	30000	No	-
SST	30000	No	-
Mod. Model	15000	No	-
Mod. Model	30000	Yes	185
Experiment (Foeth *et al.*, 2006)	-	-	152

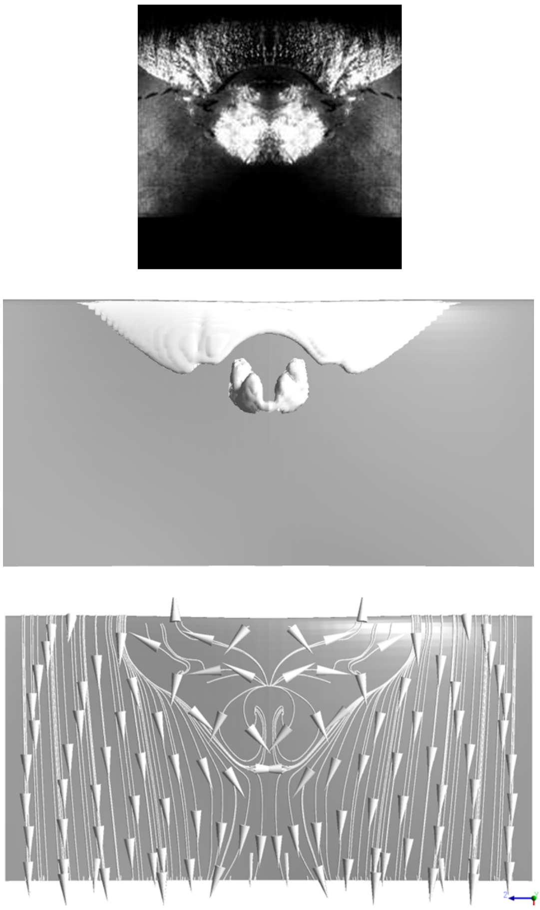

Figure 7. Flow behavior results compared with experiment (Foeth and Terwisga, 2006).

while, the new cavity started to form at the leading edge of blade to replace the condensed one constantly in each period of time.

Concerning characteristics of cavitating flow at the leading edge of this blade, cavity tends to form near the shroud than the hub. Due to configuration of blade geometry and centrifugal force, the flow direction near the blade surface tends to move from the hub to the shroud wall resulting in the formation of cavities. Besides, vortices also occur near the shroud, (Figure 9).

The structure of cavities is broken off by a vortex and shedding the vapor cloud downstream near the shroud wall. Periodically, the shape of shedding cavities is horse-shoe like because the influence of downstream flow has high vorticity. This pattern of flow is called “cavitation vortex” (Grekula and Bark, 2001).

Dynamic changes of cavity over time are demonstrated in Figure 10. Cavities start to form at leading edge on suction side of the blade affected by vortex leading to break off the cavities. The small break-up ones are shedding and transported downstream. While the first cavities are shedding, the main cavities attached to the blade surface start to reform continuously. When shedding cavities are reaching to the higher pressure region, they will be condensed. The condensed cavities occurring at trailing edge of the blade surface may damage the blade itself resulting in shortening of its life time (Klein, 1974).

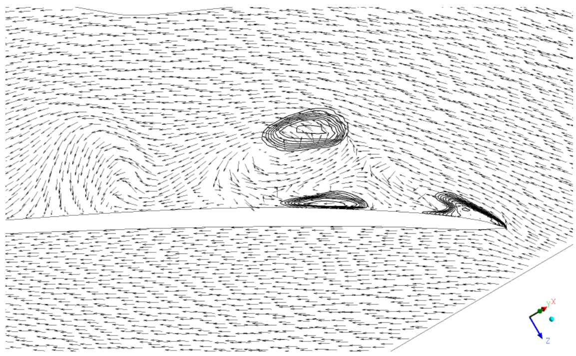

Figure 8. Velocity vector plot on a blade section at span 5% from the shroud wall.

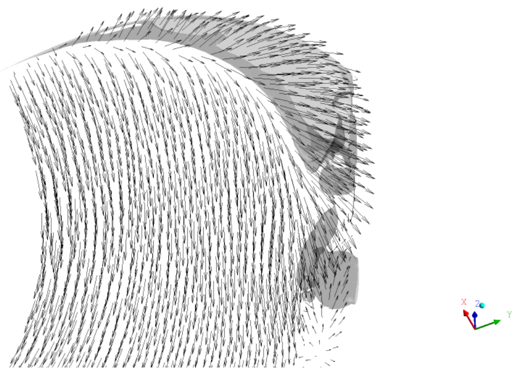

Figure 9. Velocity vector plot at the blade surface.

Table 3. Flow behaviors that can be captured by this research.

Grekular and Bark (2001) – Experimental method Flow behaviors	This research – Numerical method Results can capture the behaviors
Re-entrant Jet	Yes
Cavity formation	Yes
Cavitation Vortices	Yes

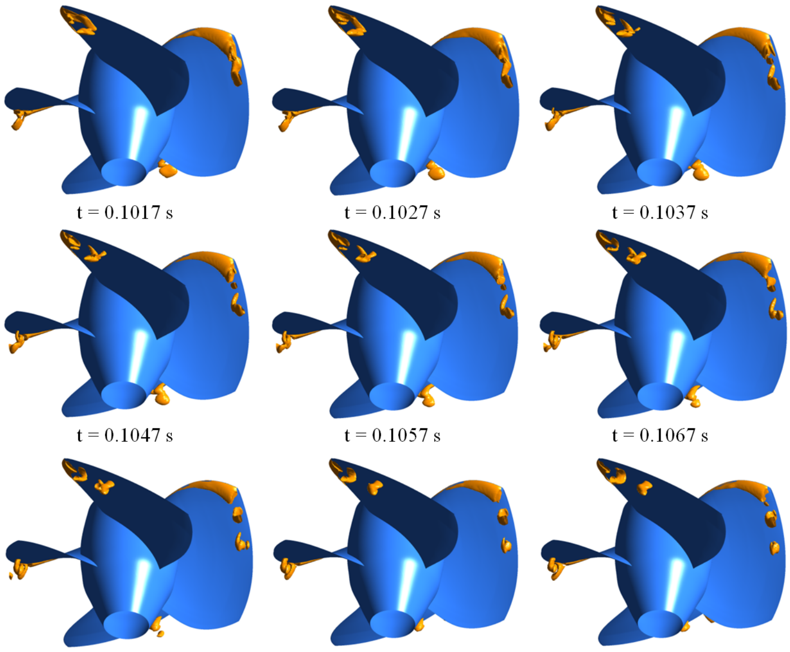

Figure 10. Dynamic change of cavities at the leading edge of the blade at each time.

Rate of shedding cavities is obtained by vapor area fraction on blade versus time graph (Figure 11). Changes of vapor area fraction over time are observed, which explain changes of cavities. As the size of cavities is increasing, the vapor area fraction on blade is increasing. The vortex, due to separation, starts to flow to the cavity structure and breaks off into smaller parts, some cavities from the break-up are shedding downstream and the others, which remain attached to the blade, are decreasing in size. This explains why the vapor area fraction on blade is also decreasing.

Figure 12 shows the variation of torque on blade over time, which is around 440-580 Nm according to the graph. This variation can be explained by fluctuation of pressure. While pressure is decreasing due to the formation of cavities at the leading edge on suction side, the pressure difference between suction and pressure side of blade will increase and torque will also increase. On the other hand, when pressure is increasing due to shedding cavities and collapsing of vapor cloud, the pressure difference between suction and pressure side of blade will decrease and a torque will also decrease.

To obtain the relationship between vapor area fraction and torque on blade, we used the Fast Fourier Transform (FFT) method to calculate and plot graph between power spectrum density and frequency as shown in Figure 13 and 14.

Based on the results from FFT of vapor area fraction, we found that the maximum power spectrum density was in low frequency range. So, the shedding frequency of cavity, which was about 46 Hz, was also in the low frequency range. From Figure 14, we found that the power spectrum density calculated by FFT of torque on blade is related to FFT of

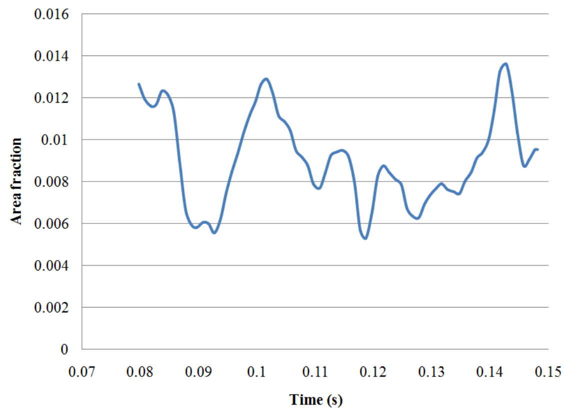

Figure 11. Change of vapor area fraction on blade over time.

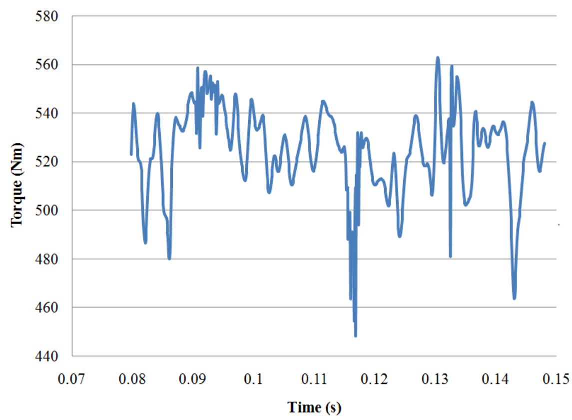

Figure 12. Change of torque on blade over time.

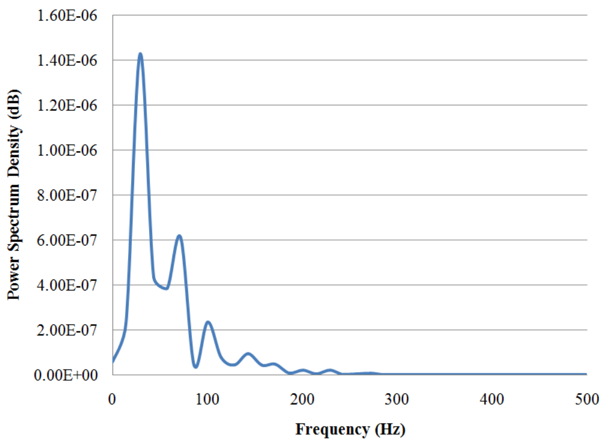

Figure 13. FFT of vapor area fraction on blade.

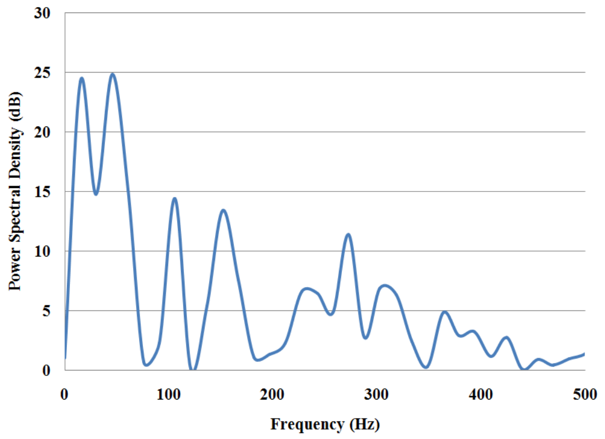

Figure 14. FFT of torque on blade.

vapor area fraction on blade in a low frequency range or a range of shedding frequency. The relationship of two figures demonstrated that the shedding frequency had effects on fluctuation of torque on blade. However, torque fluctuation was also found in a higher frequency range, which might be explained by the influence of high turbulence on a pressure side of blade.

The effect of torque fluctuation on water turbine blades resulted in the occurrence of vibration at blade leading to shortening of water turbine's life time and generation of noise pollutions (Avellan, 2004).

11. Conclusions

A new k-ω turbulent model for unsteady cavitation flow has been developed. The turbulent Mach number including an effect of compressibility was calculated with volume fraction. A modified k-ω code was added to the program in order to improve β and β^* accurately. The simulation results with new modified k-ω turbulent model gave clearly cavity shedding characteristic. A comparison with both two and three dimensional hydrofoils, it is found that this modified model can be used to simulate unsteady flow behaviors correctly when compared with experimental results (Arndt *et al.*, 2000), (Foeth and Terwisga, 2006) and is better than the available model.

The computational results have shown a capability of unsteady cavitation flow behaviors prediction on 3-D runner turbine, including re-entrant jet, cavity shedding, cavitation vortices, and periodical behavior of cavitation flow. When fluid flows through the turbine, the cavity occurs and attach to the blade surface at the leading edge and suction side of runner turbine. Re-entrant jet is an important mechanism that causes the cavity shed to the downstream. Some parts of the shedding cavity are similar to horseshoe shape due to the influence of vortices at the trailing edge, called cavitation vortices. While the old cavity was shedding from the leading edge, the new was formed instead. This periodically repeat is called cavitation cycle. The cycle frequency, 46 Hz was found by performing FFT analysis on torque variation and evolution of vapor area on blade surface at the normal operation of this turbine.

The fluctuation of torque on blade during an operation is a major cause of reducing water turbine's life time. These factors should be taken into serious consideration by turbine designers.

References

Arndt, R.E.A., Song, C. C. S., Kjeldsen, M., He, J., and Keller, A. P. 2000. Instability of Partial Cavitation: A Numerical/Experimental Approach. Proceedings of Twenty-Third Symposium on Naval Hydrodynamics, National Academies Press, Val de Reuil, France.

Avellan, F. 2004. Introduction to Cavitation in Hydraulic Machinery. Proceedings of The Sixth International Conference on Hydraulic Machinery and Hydrodynamics., Timisoara Romania, October 21-22, 2004.

Barth, T. and Jesperson, D. 1989. The Design and Application of Upwind Schemes on Unstructured Meshes. American Institute of Aeronautics and Astronautics 27th Aerospace Sciences Meeting, Reno, Nevada, 1989, Technical Report AIAA-89-0366.

CFX-ANSYS, L.C. 2004. CFX-5.7: Solver Theory, ANSYS Inc., Canada.

Coutier-Delgosha, O., Fortes-Patella, R., and Reboud, J. L. 2003. Evaluation of the Turbulence Model Influence on the Numerical Simulations of Unsteady Cavitation. Trans of the American Society of Mechanical Engineers, 125, 38-45.

Foeth, E.J., and Terwisga, T.V. 2006. The Structure of Unsteady Cavitation. Part 1: Observations of an Attached Cavity on a Three-Dimensional Hydrofoil. Proceedings of the Sixth International Symposium on Cavitation. (CAV2006), Wageningen, Netherland.

Franc, J.P., and Michel, J. M. 2004. Fundamentals of Cavitation. Kluwer Academic Publishers, U.S.A., pp. 131-144.

Grekula, M., and Bark, G. 2001. Experimental Study of Cavitation in a Kaplan Model Turbine. Proceedings of the Fourth International Symposium on Cavitation (CAV 2001). California Institute of Technology, Pasadena, California, U.S.A., June 20-23, 2001.

Klein, J. 1974. Cavitation problems on Kaplan runners. In Cavitation. Fluid Machinery Group of the Institution of Mechanical Engineers, Heriot-Watt University, Edinburgh, Scottland, 303–308.

Koop, A.H. 2008. Numerical Simulation of Unsteady Three-Dimensional Sheet Cavitation, Unpublished PhD Thesis, University of Twente, Netherlands, pp.131-173.

Kubota, A., Kato, H., and Yamaguchi, H. 1992. A new Modelling of Cavitating Flows : A Numerical Study of Unsteady Cavitation on a Hydrofoil Section. J. Fluid Mech. 240, 59-96.

Tiaple, Y., and Nontakaew, U. 2004. The Development of Bulb Turbine for Low Head Storage Using CFD Simulation. National Research Council of Thailand (NRCT).

Wilcox, D. 2004. Turbulence Modeling for CFD, DCW Industries, Inc., La Canada, California, U.S.A., pp.171-188.

Abbreviation

A = Speed of sound in fluid
$\vec{C}$ = Velocity vector
F = Constant
$\vec{f}$ = External force vector
k = Turbulent kinetic energy
M = Mach number
$\overrightarrow{M}$ = Momentum force vector
$\dot{m}$ = Mass flow rate
N = Number of bubbles
p = Pressure
R = Bubble radius
$\vec{r}$ = Vector value from upwind node
α = Volume fraction, Alpha coefficient
β, β^* = Beta and Beta star coefficient, Constant
ε = Dissipation
μ = Viscosity of fluid
$\underline{\sigma}$ = Turbulent Schmidt number
τ = Shear stress tensor
ϕ = Node value
ω = Turbulent dissipation rate

Subscripts

d = Dilatation
i = Initial
l = Liquid phase
n = n^{th} phase
nuc = Nucleation
o = Nuclide
t = Turbulence
s = Solenoidal
v = Vapor
w = Water

Superscripts

c = Condensation
v = Vaporization